JLAB-THY-15-xxxx

Constraints on large-x parton distributions from new weak boson production and deep-inelastic scattering data

(Dated: August 25, 2015)

Abstract

We present a new set of leading twist parton distribution functions (PDFs), which take advantage of developments in the theoretical treatment of nuclear corrections as well as new data. The analysis includes for the first time data on the free neutron structure function from the BONuS experiment at Jefferson Lab, and new charged lepton and W-boson asymmetry data from Fermilab, which significantly reduce the uncertainty on the d/u ratio at large values of x.

I. INTRODUCTION

[XXX editing]

... general intro ...

... what is new since CJ12 ...

• more complete/consistent/systematic treatment of nuclear corrections esp. nucleon off-shell corrections

• impact of new W-boson asymmetry data on d/u ratio

• inclusion of JLab (BONuS) data

• analysis of $\bar{d} - \bar{u}$ at large x ... choose either $\bar{d}/\bar{u} \to 1$ or 0 as $x \to 1$ ...

• S-ACOT scheme for heavy quarks

• LO fit

• α_s treatment

... In Sec. II we ...

II. THEORETICAL FOUNDATIONS

In this section we present the theoretical framework that is used for the CJ15 analysis.

A. PDF parametrizations [XXX editing]

• For the parametrization of the PDFs at the input scale Q_0^2, a common form has been adopted for all parton species f,

$$xf(x, Q_0^2) = a_0 x^{a_1} (1-x)^{a_2} (1 + a_3 \sqrt{x} + a_4 x). \tag{1}$$

This form applies to the valence distributions $xq_v \equiv x(q - \bar{q})$, for $q = u$ and d, the isoscalar and isovector sea quark distributions $x(\bar{u} + \bar{d})$ and $x(\bar{d} - \bar{u})$, and the gluon distribution xg. However, to allow for a more flexible parametrization of the valence d_v PDF in the large-x region, we add in a small admixture of the u_v PDF,

$$d_v \to a_0^{d_v} \left(\frac{d_v}{a_0^{d_v}} + b\, x^c u_v \right), \tag{2}$$

with b and c as two additional parameters. The result of this modification is that $d_v/u_v \to a_0^{d_v}\, b$ as $x \to 1$, provided $a_2^{d_v} > a_2^{u_v}$, which is usually the case. A finite, nonzero value of this ratio is indeed expected in several nonperturbative models of hadron structure [6–8]. It is also required from a purely practical point of view, as it avoids potentially large biases on the d-quark PDF central value [14], as well as on its PDF error estimate, as we discuss in detail in Sec. IV. The a_0 parameters for the u_v and d_v distributions are fixed by the appropriate valence quark number sum rules, while a_0^g is fixed by the momentum sum rule.

- For the input scale Q_0 we choose the charm quark scale, $Q_0 = m_c$.
- New parametrization for $\bar{d} - \bar{u}$ ... avoids negative PDFs? ...

In our analysis we parametrize the $\bar{d}/\bar{u}$ ratio as

$$\frac{\bar{d}}{\bar{u}} = a_0 x^{a_1}(1-x)^{a_2} + 1 + x^{a_3}(1-x)^{a_4}, \tag{3}$$

which ensures that in the limit $x \to 1$ one has $\bar{d}/\bar{u} \to 1$. The existing data are not able to reliably determine the large-x behavior of the ratio, so as an alternative we also perform fits using $\bar{d}/\bar{u} = a_0 x^{a_1}(1-x)^{a_2} + (1 + x^{a_3})(1-x)^{a_4}$, which vanishes in the $x \to 1$ limit. The $\bar{d}/\bar{u} \to 1$ limit is what would be expected from perturbative QCD, while the $\bar{d}/\bar{u} \to 0$ limit may arise if the trend in $x \gtrsim 0.3$ points from the E866 experiment [28] were to continue to larger x.

- The strange quark distribution is not well constrained by existing data ...[SOME DISCUSSION OF ISSUES]... For the strange quark PDF, we follow our previous analyses [14, 15] by assuming flavor independence of the shape of the sea quark PDFs, and consequently take a fixed ratio

$$\kappa = \frac{s + \bar{s}}{\bar{u} + \bar{u}}, \tag{4}$$

with the further assumption that $\bar{s} = s$. In this study we take $\kappa = 0.4$.

B. Heavy quarks [JFO?? editing]

- Implementation of S-ACOT scheme.
- In our analysis we take the masses of the charm and bottom quarks to be $m_c = 1.3$ GeV and $m_b = 4.5$ GeV, respectively.
- The 4-flavor value of the QCD cutoff scale used in this analysis is $\Lambda_{\rm QCD}^{(4)} = 226.8$ MeV.

C. $1/Q^2$ corrections [XXX editing]

• For target mass corrections, use of OPE (G-P); ... comparisons with EFP, series expansion; ... in practice doesn't matter!(?)

• For other subleading $1/Q^2$ corrections, such as higher twist and other residual power corrections (

• ... anything different to CJ12??

$$F_2(x, Q^2) = F_2^{\rm LT}(x, Q^2)\left(1 + \frac{C(x)}{Q^2}\right), \tag{5}$$

where $F_2^{\rm LT}$ denotes the leading twist structure function including TMCs. For simplicity we generically refer to the fitted $1/Q^2$ term as a "higher twist" correction, and parametrize the higher twist coefficient function by

$$C(x) = h_0 x^{h_1}(1 + h_2 x), \tag{6}$$

assuming it to be isospin independent (see, however, Refs. [60–63]).

D. Nuclear corrections [WM editing]

• The analysis includes nuclear corrections for deuterium account for nucleon Fermi motion and nuclear binding effects, which are implemented using nuclear smearing functions, as well as rescattering effects mediated by Pomeron and meson exchange mechanisms which give rise to shadowing at small $x \lesssim 0.1$ and a small amount of antishadowing at $x \sim 0.1$. For the shadowing and antishadowing corrections, the model of Ref. [1] is used (see also Refs. [2, 3]), although the effects of these is negligible in our analysis.

The implementation of the nuclear smearing is performed ... ...

1. Nuclear smearing [WM editing]

Since nucleons bound in a nucleus are not free, the nuclear structure function deviates from a simple sum of free proton and neutron structure functions, especially at large x where the effects of Fermi motion, nuclear binding, and nucleon off-shellness are most prominent. In the nuclear impulse approximation the structure function of the deuteron d can be expressed as a generalized convolution of the bound nucleon structure function and a momentum distribution $f_{N/d}$ of nucleons in the deuteron [64, 65],

$$q^d(x,Q^2) \;=\; \int \frac{dz}{z} dp^2\, f_{N/d}(z,p^2)\, \widetilde{q}^N(x/z,p^2,Q^2), \tag{7}$$

where $f_{N/d}(z,p^2)$ gives the (light-cone) distribution of nucleons in the deuteron for a given nucleon momentum fraction in the deuteron $z = (M_d/M)(p\cdot q/p_d\cdot q)$ and nucleon virtuality p^2, where p and p_d are the four-momenta of the nucleon and deuteron, respectively, and M_d is the deuteron mass. The function $\widetilde{q}^N$ is the off-shell nucleon structure function, and a sum over the nucleons $N = p, n$ is implied. ... The function $\widetilde{q}^N$ includes $1/Q^2$ corrections, such as TMCs and higher twist effects. ... Expanding the off-shell nucleon structure function about the on-shell limit, one finds [66]

$$\widetilde{q}^N(x,p^2,Q^2) \;=\; q^N(x,Q^2)\left(1+\frac{p^2-M^2}{M^2}\delta f^N(x,Q^2)\right), \tag{8}$$

where the coefficient of the off-shell term is

$$\delta f^N(x,Q^2) \;=\; \left.\frac{\partial \ln \widetilde{q}^N(x,p^2,Q^2)}{\partial \ln p^2}\right|_{p^2=M^2}, \tag{9}$$

and the $\widetilde{q}^N$ includes the parametrized higher twist corrections of Eq. (5). The on-shell term leads to the standard on-shell convolution representation for the nuclear structure function, while the off-shell term can be evaluated as an additive correction, $q^d = q^{d\,(\mathrm{on})} + q^{d\,(\mathrm{off})}$, where

$$q^{d\,(\mathrm{on})}(x,Q^2) \;=\; \int \frac{dz}{z} f^{(\mathrm{on})}(z)\, q^N(x/z,Q^2), \tag{10a}$$

$$q^{d\,(\mathrm{off})}(x,Q^2) \;=\; \int \frac{dz}{z} f^{(\mathrm{off})}(z)\, \delta f^N(x/z,Q^2)\, q^N(x/z,Q^2). \tag{10b}$$

The on-shell and off-shell smearing functions $f^{(\mathrm{on})}$ and $f^{(\mathrm{off})}$ are taken to be the same for the proton and neutron, and are given by [68]

$$f^{(\mathrm{on})}(z) \;=\; \int dp^2\, f_{N/d}(z,p^2), \tag{11a}$$

$$f^{(\mathrm{off})}(z) \;=\; \int dp^2\, \frac{p^2-M^2}{M^2}\, f_{N/d}(z,p^2). \tag{11b}$$

The momentum distributions, or "smearing functions", $f^{(\mathrm{on})}$ and $f^{(\mathrm{off})}$, are computed in the weak binding approximation (WBA) in terms of the deuteron wave function, and include the effects of nuclear binding and Fermi motion [66, 67]. At $Q^2 \to \infty$ the on-shell smearing function $f^{(\mathrm{on})}$ has a simple probabilistic interpretation in terms of the light-cone momentum fraction $z \approx (M_d/M)(p^+/p_d^+)$ of the deuteron carried by the struck nucleon, while at finite Q^2 it depends in addition on the parameter $\rho^2 = 1 + 4x^2M^2/Q^2$, which characterizes the deviation from the Bjorken limit.

The nuclear corrections at large x depend partly on the strength of the high-momentum tail of the deuteron wave function, and we use several wave functions based on different nucleon–nucleon potentials to study the deuteron model dependence. We choose the high-precision AV18 [69], CD-Bonn [70] and the relativistic WJC-1 and WJC-2 [71] wave functions, which provide a representative spread of behaviors at high momentum. Note that the effects of the nuclear smearing corrections are not suppressed at large Q^2, and must be considered at all scales wherever data at $x \gtrsim 0.3$ are used [11–13].

• Same off-shell functions in DIS and DY.

2. *Nucleon off-shell corrections [WM editing]*

• The off-shell nucleon correction $\delta^{(\mathrm{off})}q^d$ is somewhat more model dependent, but several quark model based estimates of this have been made in the literature [66, 72, 73].

• ... give brief history of off-shell corrections

- MST (theoretical)

- KP (model/fitted)

- CJ11 (mKP)

- CJ12 (more consistent mKP)

- CJ15 (calculation at parton level - different treatment of valence quarks, antiquarks and gluons - can apply to any observable, not just F_2 structure function - in CJ11 and CJ12 had used overall multiplicative constant, only for F_2)

• In Ref. [14] this was computed using the "modified Kulagin-Petti" model. In this model, the corrections were related to the change in the nucleon's confinement radius in the nuclear medium, as well as the average virtuality of the bound nucleons, and constrained to give no net change in the structure function normalization. In contrast to Ref. [14], however, here we further take into account the correlation between the nucleon "swelling" and the deuteron wave function. The combined effects introduce a theoretical uncertainty in the extracted PDFs, particularly for the d quark.

• In CJ15 have freed off-shell parameters, allowing them to be determined by the fit. Using either fmKP model (rescaling parameter λ), or in phenomenological fit.

• In this analysis, we explore the possibility of antishadowing in the deuteron, suggested in the global nuclear analysis of KP [66], in which the F_2^d/F_2^N ratio is slightly enhanced (above unity) at $x \approx 0.1-0.2$. To allow for one or more zero crossings in the function δf^N, we use the same parametrization as in Ref. [66],

$$\delta f^N \; = \; C_N(x-x_0)(x-x_1)(1+x_0-x), \tag{12}$$

but fit the parameters to the deuterium data. The requirement that the off-shell correction does not modify the number of valence quarks in the nucleon provides the constraint

$$\int_0^1 dx\, \delta f^N(x)\, (q(x)-\bar{q}(x)) \; = \; 0. \tag{13}$$

In practice we fit the zero crossing parameter x_0 and the normalization C_N, which then allows the second zero crossing x_1 to be determined from Eq. (13) analytically.

E. PDF Errors [AA/JFO?? editing]

... as for CJ12 ... Hessian ... tolerance ...

III. DATA

[XXX editing]

The CJ15 PDFs are obtained by fitting to a global database of 4035 data points from a variety of high energy scattering processes, listed in Table I. These include deep-inelastic scattering data from BCDMS, NMC, SLAC, HERA and Jefferson Lab (JLab); Drell-Yan p and d cross sections from fixed target experiments at Fermilab; W and Z asymmetries, as well as jet and γ+jet cross sections from the CDF and DØ collaborations at the Tevatron. The table also lists the corresponding χ^2 values for each data set. The overall χ^2/dof is 0.979. The fit is slightly better than in our previous CJ12 analysis [15], partly because of the greater flexibility which we have allowed in the current fit for the nucleon off-shell correction.

...[FURTHER DESCRIPTIONS OF DATA]... ...[JUSTIFICATION FOR INCLUDING AND OMITTING SPECIFIC DATA SETS]...

IV. RESULTS

[WM editing]

In this section we present the results of our global QCD analysis. The quality of the fit to data is illustrated in Figs. 1 and 2, where the inclusive F_2 structure functions of the proton and deuteron are compared with the CJ15 calculations over several decades of Q^2 and x. For the proton F_2^p structure function in Fig. 1, data from BCDMS [22], NMC [23], SLAC [25] and JLab [26] experiments are shown at approximately constant values of x, while for the JLab data (see inset in Fig. 1) the structure functions are presented at fixed scattering angles, with x increasing with Q^2. The agreement for all the sets is excellent ...[???]..., with the exception of ...[???]...

Similar agreement is seen for the deuteron F_2^d structure function in Fig. 2, where measurements from BCDMS [22], SLAC [25] and JLab [26] are compared with the CJ15 results (data from NMC are presented as a ratio to the proton structure function, F_2^d/F_2^p). ...[SHOW OTHER, e.g. HERA, DATA SEPARATELY??]...

A. CJ15 PDFs [WM editing]

The CJ15 PDFs themselves are displayed in Fig. 3 at a scale of $Q^2 = 10$ GeV^2 for the u, d, $\bar{d}+\bar{u}$ and $\bar{d}-\bar{u}$ distributions, and the gluon distribution scaled by a factor 1/10. The central CJ15 PDFs are determined using the AV18 deuteron wave function and the nucleon off-shell parametrization in Eq. (12), with the parameter values and their errors for the leading twist distributions given in Table II. at the input scale Q_0^2. The uncertainty bands on the PDFs correspond to $\Delta\chi^2 = 1$. The parameters without errors have been fixed by sum rules or other constraints. (To avoid rounding errors when using these values in numerical calculations, we give the parameter values to 5 significant figures.) PDFs for other flavors, such as strange and charm, are not shown in Fig. 3. The strange quark PDF is assumed to be proportional to the light antiquark sea in the ratio $\kappa = 0.4$ [see Eq. (4)], while the charm quark distribution is generated perturbatively through Q^2 evolution. While there has been speculation about nonperturbative or intrinsic contributions to PDFs of heavy flavors, there is currently no evidence from global analysis of high energy scattering data to suggest that these are large [87]. Until more conclusive evidence becomes available, in this analysis we follow the conventional approach in setting these to zero. This is in contrast with the light quark sea, for which a nonperturbative component at the input scale is essential to account for the nonzero flavor asymmetry $\bar{d} - \bar{u}$. ...[NOTE VERY ASYMMETRIC ERRORS AT SMALL x]...

The CJ15 PDFs are compared with PDFs from several recent representative NLO global parametrizations in Fig. 4, in the form of ratios to the central CJ15 distributions. Since different PDF analyses typically utilize different criteria for estimating PDF errors, we display the CJ15 errors for the standard $\Delta\chi^2 = 1$ (or tolerance $T = 1$), as well as with errors inflated by a tolerance of $T = 10$ [15]. Generally the MMHT14 [17] and NNPDF3.0 [19] PDF sets have uncertainties that are comparable to the CJ15 PDF errors with $T = 10$, while those for the HERAPDF15 [21] distributions are closer to the CJ15 $T = 1$ errors. This may be expected given that the HERAPDF15 analysis only fits HERA data, and therefore uses the $\Delta\chi^2 = 1$ criterion for generating errors.

As known from most previous analyses, the relative uncertainties on the d-quark PDFs are significantly larger than those on the u-quark PDF, especially at large x. For the $\bar{u}$ and $\bar{d}$ distributions the results from the CJ15 fit are similar to those from the MMHT14 and NNPDF3.0 analyses, while the HERAPDF15 fit gives significantly different results beyond $x \approx 0.1 - 0.2$. Note that the $\bar{d}/\bar{u}$ ratio is most strongly constrained by the E866 Drell-Yan pp and pd scattering data. For the strange quark PDF, the uncertainties in CJ15 are somewhat smaller than in MMHT14 and NNPDF3.0. This is mostly due to the fact that the CJ15 s-quark PDF is assumed to scale with the light antiquark sea in the ratio $\kappa = 0.4$, while other analyses attempt to constrain s-quark PDF from neutrino data, which typically have much larger uncertainties. The errors on the gluon distribution in the MMHT14 and NNPDF3.0 fits lie somewhere between the $T = 1$ and $T = 10$ CJ15 errors, while the HERAPDF15 uncertainties are comparable to the $T = 1$ CJ15 results, as was the case for the various quark distributions. Uncertainties in other modern PDF analyses, such as CT14, ABM, ... are generally between the representative sets illustrated in Fig. 4. ...[ANY OTHER COMMENTS ABOUT THE GENERAL FEATURES/ERRORS?]...

B. Nuclear corrections at large x [WM editing]

As observed in Fig. 4, the uncertainty on the d-quark distribution at large x values ($x \gtrsim 0.3$) is generally much larger compared with that on the u-quark PDF. This reflects the considerable greater quantity of high precision proton F_2^p structure function data, which, because of the larger charge on the u quark, is at least an order of magnitude more sensitive to the u-quark PDF than to the d. Traditionally, stronger constraints on the d-quark PDF have been sought from inclusive DIS from the neutron, in which the roles of the u and d quark are reversed relative to the proton. However, the absence of free neutron targets has meant that neutron structure information has had to be extracted from measurements on deuterium nuclei. Unfortunately, at high values of x ($x \gtrsim 0.5$) bound state effects in the deuteron become important, and uncertainties in their computation become increasing large with increasing x.

The effects of nuclear corrections on the PDFs are illustrated in Fig. 5, where fits using several different deuteron wave function models are compared. The distributions are displayed relative to the central CJ15 PDFs which use the AV18 deuteron wave function. All fits employ the phenomenological nucleon off-shell parametrization in Eq. (12), with the parameters given in Table III for the AV18 deuteron wave function. The results using the CD-Bonn or WJC-2 wave function are very similar to those for the AV18 wave function, while using the WJC-1 model leads to larger differences. In fact, the AV18 and CD-Bonn models give almost identical total χ^2/dof of 0.979, while the WJC-2 model gives 0.980, making these three fits essentially indistinguishable. This suggests that, for the most part, the nucleon off-shell parametrization in Eq. (12) is sufficiently flexible to compensate for changes induced by these wave functions. For the WJC-1 model, which has the hardest momentum distribution, it is more difficult for the off-shell correction to compensate within the constraints of Eq. (12), and this leads to a slightly worse overall fit, with a χ^2/dof value of 0.983.

As expected, the variations due to the nuclear models have the largest effects in the d-quark distribution, which is less constrained by proton data and hence more sensitive to uncertainties in the extracted neutron structure function. The spread in the d PDF at $x = 0.8$ is $\approx 20\%$ for all four wave functions. The variations for the AV18, CD-Bonn and WJC-2 wave functions are generally within the $\Delta\chi^2 = 1$ confidence limit, while the WJC-1 results lie outside the band for the u and d PDFs. In particular, the d-quark PDF for the WJC-1 deuteron model is suppressed at high x relative to that in the other models, which correlates with the harder smearing function $f_{N/d}$ at large values of the nucleon light-cone momentum y and hence a larger F_2^d/F_2^N ratio at high x. Interestingly, one also observes an anti-correlation between the behavior of the d-quark distribution at large x and the gluon distribution. In fact, using the WJC-1 wave functions leads to slight decreases in all the quark PDFs at high x, while the gluon PDF has the opposite trend. The spread in the gluon PDF is $\lesssim 10\%$ for $x < 0.8$, although beyond $x \approx 0.3$ the gluon distribution has a very large uncertainty.

Note that while in Fig. 5 the same functional form from Eq. (12) is used for all fits, the off-shell parameters are refitted for each different deuteron wave function model. The fitted off-shell functions δf^N are shown in Fig. 6 for the four wave function models considered. The off-shell corrections for the AV18, CD-Bonn and WJC-2 models have similar shapes: quite small at low x but becoming more positive at larger x. The function δf^N for these models has zero crossings at $x = x_1 \approx 0.05$ and $x = x_0 \approx 0.3$. For the WJC-1 model, on the other hand, the off-shell function is similar in magnitude, but has a shape that is somewhat orthogonal to the others. In this case it becomes more negative for $x \gtrsim 0.5$, with the parameter $x_1 \approx 0.15$, while the other zero crossing parameter is negative, $x_0 \approx -0.25$.

To test the sensitivity of the fit to the off-shell model, we also consider a somewhat different prescription for the off-shell correction δf^N, along the lines of that adopted in our previous analyses [14, 15] (see also Ref. [66]). Namely, we express the PDF through a spectral representation, in terms of a quark spectral function characterized by an ultraviolet momentum cutoff scale Λ and an invariant mass of the "diquark" system (proton with a quark removed) that is spectator to the deep-inelastic collision. The spectator mass is fixed by comparing with the on-shell proton structure function data, and the variation of the scale Λ with the nucleon virtuality p^2 may be interpreted within a valence approximation as a rescaling of the nucleon confinement radius [66]. To apply the model to observables that are sensitive to both the valence and sea quark sectors, in the present analysis we generalize the single-pole approximation to the spectral function to allow different off-shell behaviors of the valence, sea quark and gluon distributions. The three corresponding spectator state masses ("qq" for valence quarks, "$qq\bar{q}$" for sea quarks, and "qqq" for gluons) are then fitted to the isoscalar valence, sea quark and gluon PDFs in the free nucleon. The rescaling parameter

$\partial \log \Lambda^2 / \partial \log p^2$ at $p^2 = M^2$ is then included as a parameter in the fit, with errors propagated along with those of the other fit parameters in Tables II and III.

The results of the fit within this model, which we refer to as the off-shell covariant spectator (OCS) model, are displayed in Fig. 7 for various PDFs as ratios to the central CJ15 PDFs (computed using the off-shell parametrization (12) and the AV18 deuteron wave function). For the AV18, CD-Bonn and WJC-2 wave functions, the effects of the more restrictive OCS model (which involves one off-shell parameter instead of three for the parametrization in Eq. (12) and relatively small and generally within the $\Delta\chi^2 = 1$ bands. The overall χ^2/dof value is 0.982 for both the AV18 and CD-Bonn wave functions, and 0.984 for the WJC-2 wave function. This is marginally higher than the results of the fit with the phenomenological off-shell parametrization in Eq. (12), and comes mostly from a slightly higher χ^2 values for the SLAC F_2^d and DØ charged lepton asymmetry data. For the WJC-1 wave function, the results for the d-quark PDF show significantly greater deviation at large x, again suggesting that the hard tail of its momentum distribution is difficult to accommodate also within the OCS model, with a total χ^2/dof of 0.989. In addition, for the u-quark distribution the WJC-1 result lies slightly outside the uncertainty band at $x \sim 0.05$.

...[WM EDITING]...

We should note at this point that ... ... off-shell corrections alone are unphyiscal, in the sense that only the combination of deuteron wave function (in the smearing function) and off-shell correction affects the observable F_2^d structure function ... ... this is clearly illustrated in Fig. 8, where ... maybe F2d/F2N plots discussed here??? ... give almost identical ratios???

... as observed in our earlier study [11], there is some degree of compensation/interplay ... between the TMCs and higher twist corrections ... The parameters for the higher twist correction to F_2 in Eqs. (5) and (6) are given in Table III.

C. d/u ratio [WM editing]

The impact of the nuclear corrections and data constraints on the d/u ratio are illustrated in Figs. 10 and 13.

In Fig. 10:

- BONuS data shrink error on d/u slightly in the $x \approx 0.5 - 0.6$ range

• significant reduction in error once W asymmetry data added

• For other deuteron wave function models, the total χ^2 values are very similar, with $\chi^2/\text{dof} = 0.979$ for the CD-Bonn wave function, 0.983 for the WJC-1 wave function, and 0.980 for the WJC-2 model. The AV18, CD-Bonn and WJC-2 model fits are therefore essentially indistinguishable, while the WJC-1 model, with its significantly harder deuteron wave function, has a slightly worse overall fit.

• With the off-shell covariant spectator (OCS) model ...[WHAT WE HAD BEEN CALLING "fmKP"]..., the χ^2 values for the various wave functions are marginally higher, with $\chi^2/\text{dof} = 0.982, 0.982, 0.989$ and 0.984 for the AV18, CD-Bonn, WJC-1 and WJC-2 models. Here again the WJC-1 gives the worst fit. ...[MORE DISCUSSION]...

• impact of various data sets on d/u ratio:

- DIS only: large uncertainty

- BONuS shrinks uncertainty appreciably at $x \sim 0.6$

- lepton asymmetry data gives significant reduction in uncertainty at $0.2 \lesssim x \lesssim 0.4$, with smaller reduction at larger x

- Z rapidity data, on the other hand, has very little effect on the uncertainty

- W asymmetry data, in particular the DØ data [34], gives significant reduction in the d/u uncertainty for $x \gtrsim 0.6$

The effects of deuterium data and the nuclear corrections in the deuterium data are illustrated in Fig. 13:

- with no nuclear corrections the d/u ratio is larger at $x \gtrsim 0.6$ than with the nuclear corrections. This can be understood from the shape of the F_2^d/F_2^N ratio Fig. 8 at large x, where the effect of the nuclear corrections is to increase the ratio above unity for $x \gtrsim 0.6$. Since F_2^d and F_2^p are fixed inputs, a larger F_2^d/F_2^N is generated by a smaller neutron F_2^n and hence a smaller d/u ratio. For example, the effect of the nuclear corrections is to shift the d/u ratio at $x = 0.8$ from the ($T = 10$) range $\approx 0.1 - 0.3$ to $\approx 0 - 0.2$ once the smearing and off-shell effects are included.

- removing the deuterium data altogether increases the overall uncertainty band for $x \gtrsim 0.7$. Interestingly, the deuteron data also reduce the d/u uncertainties slightly at smaller x, $x \lesssim 0.1$.

The final CJ15 d/u results and uncertainties (for $T = 10$) can be compared with ratios obtained in other recent global PDF analyses. These are shown in Fig. 9 for the MMHT14

[17], CT14 [18] and JR14 [47] PDFs.

- JR14 uses similar experimental data sets and treatment of nuclear and finite-Q^2 corrections at large x;

- JR14 has largest uncertainty in the intermediate-x region, which may result from the recent W and lepton asymmetry data from CDF and DØ not being used;

- at large x the JR14 d/u ratio $\rightarrow 0$ from the form of their parametrization;

- CT14 range is similar

V. CONCLUSION

[XXX editing]

In this paper we have ...

Acknowledgments

We thank M. E. Christy, P. Monaghan, ... for for helpful discussions. This work was supported by the DOE contract No. DE-AC05-06OR23177, under which Jefferson Science Associates, LLC operates Jefferson Lab. The work of J.F.O. and A.A. was supported in part by DOE contracts No. DE-FG02-97ER41922 and No. DE-SC0008791, respectively.

---

[1] W. Melnitchouk and A. W. Thomas Phys. Rev. D **47**, 3783 (1993).

[2] B. Badelek and J. Kwiecinski, Nucl. Phys. **B370**, 278 (1992).

[3] L. P. Kaptari and A. Yu. Umnikov, Phys. Lett. B **272**, 359 (1991).

[4] R. P. Feynman, *Photon Hadron Interactions* (Benjamin, Reading, Massachusetts, 1972).

[5] F. E. Close, Phys. Lett. B **43**, 422 (1973).

[6] G. R. Farrar and D. R. Jackson, Phys. Rev. Lett. **35**, 1416 (1975).

[7] W. Melnitchouk and A. W. Thomas, Phys. Lett. B **377**, 11 (1996).

[8] R. J. Holt and C. D. Roberts, Rev. Mod. Phys. **82**, 2991 (2010).

[9] S. Kuhlmann *et al.*, Phys. Lett. B **476**, 291 (2000).

[10] L. T. Brady, A. Accardi, W. Melnitchouk and J. F. Owens, JHEP **1206**, 019 (2012).

[11] A. Accardi, M. E. Christy, C. E. Keppel, P. Monaghan, W. Melnitchouk, J. G. Morfin and J. F. Owens, Phys. Rev. D **81**, 034016 (2010).

[12] J. Arrington, F. Coester, R. J. Holt and T. -S. H. Lee, J. Phys. G **36**, 025005 (2009).

[13] J. Arrington, J. G. Rubin and W. Melnitchouk, Phys. Rev. Lett. **108**, 252001 (2012).

[14] A. Accardi, W. Melnitchouk, J. F. Owens, M. E. Christy, C. E. Keppel, L. Zhu and J. G. Morfin, Phys. Rev. D **84**, 014008 (2011).

[15] J. F. Owens, A. Accardi and W. Melnitchouk, Phys. Rev. D **87**, 094012 (2013).

[16] The CTEQ-Jefferson Lab (CJ) collaboration website, http://www.jlab.org/cj.

[17] L. A. Harland-Lang, A. D. Martin, P. Motylinski and R. S. Thorne, Eur. Phys. J. C **75**, 204 (2015).

[18] S. Dulat *et al.*, arXiv:1506.07443 [hep-ph].

[19] R. D. Ball *et al.*, JHEP **1504**, 040 (2015).

[20] F. D. Aaron *et al.*, JHEP **1001**, 109 (2010).

[21] V. Radescu, arXiv:1308.0374.

[22] A. C. Benvenuti *et al.*, Phys. Lett. B **223**, 485 (1989); *ibid.* B **236**, 592 (1989).

[23] M. Arneodo *et al.*, Nucl. Phys. B **483**, 3 (1997).

[24] M. Arneodo *et al.*, Nucl. Phys. B **487**, 3 (1997).

[25] L. W. Whitlow *et al.*, Phys. Lett. B **282**, 475 (1992).

[26] S. P. Malace *et al.*, Phys. Rev. C **80**, 035207 (2009).

[27] F. D. Aaron *et al.*, JHEP **1001**, 109 (2010).

[28] E. A. Hawker *et al.*, Phys. Rev. Lett. **80**, 3715 (1998); J. Webb, Ph.D. Thesis, New Mexico State University (2002), arXiv:hep-ex/0301031; P. Reimer, private communication, `http://p25ext.lanl.gov/e866/papers/e866dyabs/E866_Drell-Yan_Cross_Sections/E866_Drell-Yar`

[29] R. S. Towell *et al.*, Phys. Rev. D **64**, 052002 (2001).

[30] D. Acosta *et al.*, Phys. Rev. D **71**, 051104(R) (2005).

[31] V. M. Abazov *et al.*, Phys. Rev. D **88**, 091102 (2013).

[32] V. M. Abazov *et al.*, Phys. Rev. D **91**, 032007 (2015).

[33] T. Aaltonen *et al.*, Phys. Rev. Lett. **102**, 181801 (2009).

[34] V. M. Abazov *et al.*, Phys. Rev. Lett. **112**, 151803 (2014) [Phys. Rev. Lett. **114**, 049901 (2015)].

[35] T. Aaltonen *et al.*, Phys. Lett. B **692**, 232 (2010).

[36] V. M. Abazov *et al.*, Phys. Rev. D **76**, 012003 (2007).

[37] T. Affolder *et al.*, Phys. Rev. D **64**, 032001 (2001).

[38] T. Aaltonen *et al.*, Phys. Rev. D **78**, 052006 (2008).

[39] B. Abbott *et al.*, Phys. Rev. Lett. **86**, 1707 (2001).

[40] V. M. Abazov *et al.*, Phys. Rev. Lett. **101**, 062001 (2008).
B. Abbott *et al.*, Phys. Rev. Lett. **86**, 1707 (2001).

[41] V. M. Abazov *et al.*, Phys. Lett. B **666**, 435 (2008).

[42] D. Mason *et al.*, Phys. Rev. Lett. **99**, 192001 (2007).

[43] G. Aad *et al.*, Phys. Rev. Lett. **109**, 012001 (2012).

[44] G. Moreno *et al.*, Phys. Rev. D **43**, 2815 (1991). ...[IS THIS CORRECT REFERENCE??]...

[45] S. Alekhin, J. Blümlein and S.-O. Moch, Phys. Rev. D **86**, 054009 (2012).

[46] A. D. Martin, W. J. Stirling, R. S. Thorne and G. Watt, Eur. Phys. J. C **63**, 189 (2009).

[47] P. Jimenez-Delgado and E. Reya, Phys. Rev. D **89**, 074049 (2014).

[48] P. Jimenez-Delgado, W. Melnitchouk and J. F. Owens, J. Phys. G: Nucl. Part. Phys. **40**, 093102 (2013).

[49] J. Beringer *et al.* [Particle Data Group Collaboration], Phys. Rev. D **86**, 010001 (2012), `http://pdg.lbl.gov`.

[50] H. Georgi and H. D. Politzer, Phys. Rev. D **14**, 1829 (1976).

[51] R. K. Ellis, R. Petronzio and G. Parisi, Phys. Lett. B **64**, 97 (1976).

[52] A. Accardi and J.-W. Qiu, JHEP **0807**, 090 (2008).

[53] A. Accardi, T. Hobbs and W. Melnitchouk, JHEP **0911**, 084 (2009).

[54] I. Schienbein *et al.*, J. Phys. G **35**, 053101 (2008).

[55] L. T. Brady, A. Accardi, T. J. Hobbs and W. Melnitchouk, Phys. Rev. D **84**, 074008 (2011) [Erratum-ibid. D **85**, 039902 (2012)].

[56] F. M. Steffens and W. Melnitchouk, Phys. Rev. C **73**, 055202 (2006).

[57] F. M. Steffens, M. D. Brown, W. Melnitchouk and S. Sanches, Phys. Rev. C **86**, 065208 (2012).

[58] A. De Rújula, H. Georgi and H. D. Politzer, Phys. Rev. D **15**, 2495 (1977).

[59] A. De Rújula, H. Georgi and H. D. Politzer, Ann. Phys. **103**, 315 (1977).

[60] M. Virchaux and A. Milsztajn, Phys. Lett. B **274**, 221 (1992).

[61] S. I. Alekhin, S. A. Kulagin and S. Liuti, Phys. Rev. D **69**, 114009 (2004).

[62] J. Blümlein and H. Böttcher, Phys. Lett. B **662**, 336 (2008).

[63] J. Blümlein, Prog. Part. Nucl. Phys. **69**, 28 (2013).

[64] W. Melnitchouk, A. W. Schreiber and A. W. Thomas, Phys. Rev. D **49**, 1183 (1994).

[65] S. A. Kulagin, G. Piller and W. Weise, Phys. Rev. C **50**, 1154 (1994).

[66] S. A. Kulagin and R. Petti, Nucl. Phys. A **765**, 126 (2006).

[67] Y. Kahn, W. Melnitchouk and S. A. Kulagin, Phys. Rev. C **79**, 035205 (2009).

[68] P. J. Ehlers, A. Accardi, L. T. Brady and W. Melnitchouk, Phys. Rev. D **90**, 014010 (2014).

[69] R. B. Wiringa, V. G. J. Stoks and R. Schiavilla, Phys. Rev. C **51**, 38 (1995).

[70] R. Machleidt, Phys. Rev. C **63**, 024001 (2001).

[71] F. Gross and A. Stadler, Phys. Rev. C **78**, 014005 (2008); *ibid.* C **82**, 034004 (2010).

[72] F. Gross and S. Liuti, Phys. Rev. C **45**, 1374 (1992).

[73] W. Melnitchouk, A. W. Schreiber and A. W. Thomas, Phys. Lett. B **335**, 11 (1994).

[74] J. Pumplin *et al.*, JHEP **0207**, 012 (2003).

[75] The CTEQ collaboration website, `http://www.cteq.org`.

[76] A. D. Martin, A. J. Th. M. Mathijssen, W. J. Stirling, R. S. Thorne, B. J. A. Watt and G. Watt, Eur. Phys. J. C **73**, 2318 (2013).

[77] A. Accardi, AIP Conf. Proc. **1369**, 210 (2011).

[78] D. Stump *et al.*, JHEP **0310**, 046 (2003).

[79] J. Anderson [LHCb Collaboration], arXiv:1109.3371 [hep-ex].

[80] D. d'Enterria and J. Rojo, Nucl. Phys. **B860**, 311 (2012), arXiv:1202.1762[hep-ph].

[81] Y. Liang *et al.* [Jefferson Lab Hall C E94-110 Collaboration], arXiv:nucl-ex/0410027.

[82] P. Monaghan, A. Accardi, M. E. Christy, C. E. Keppel, W. Melnitchouk and L. Zhu, Phys. Rev. Lett. **110**, 152002 (2013).

[83] N. Baillie *et al.*, Phys. Rev. Lett. **108**, 142001 (2012); S. Tkachenko *et al.*, Phys. Rev. C **89**, 045206 (2014).

[84] Jefferson Lab Experiment C12-10-103 [MARATHON], G. G. Petratos, J. Gomez, R. J. Holt and R. D. Ransome, spokespersons.

[85] Jefferson Lab Experiment E12-10-102 [BONUS12], S. Bültmann, M. E. Christy, H. Fenker, K. Griffioen, C. E. Keppel, S. Kuhn and W. Melnitchouk, spokespersons.

[86] Jefferson Lab Experiment E12-10-007 [SoLID], P. Souder, spokesperson.

[87] P. Jimenez-Delgado, T. J. Hobbs, J. T. Londergan and W. Melnitchouk, Phys. Rev. Lett. **114**, 082002 (2015).

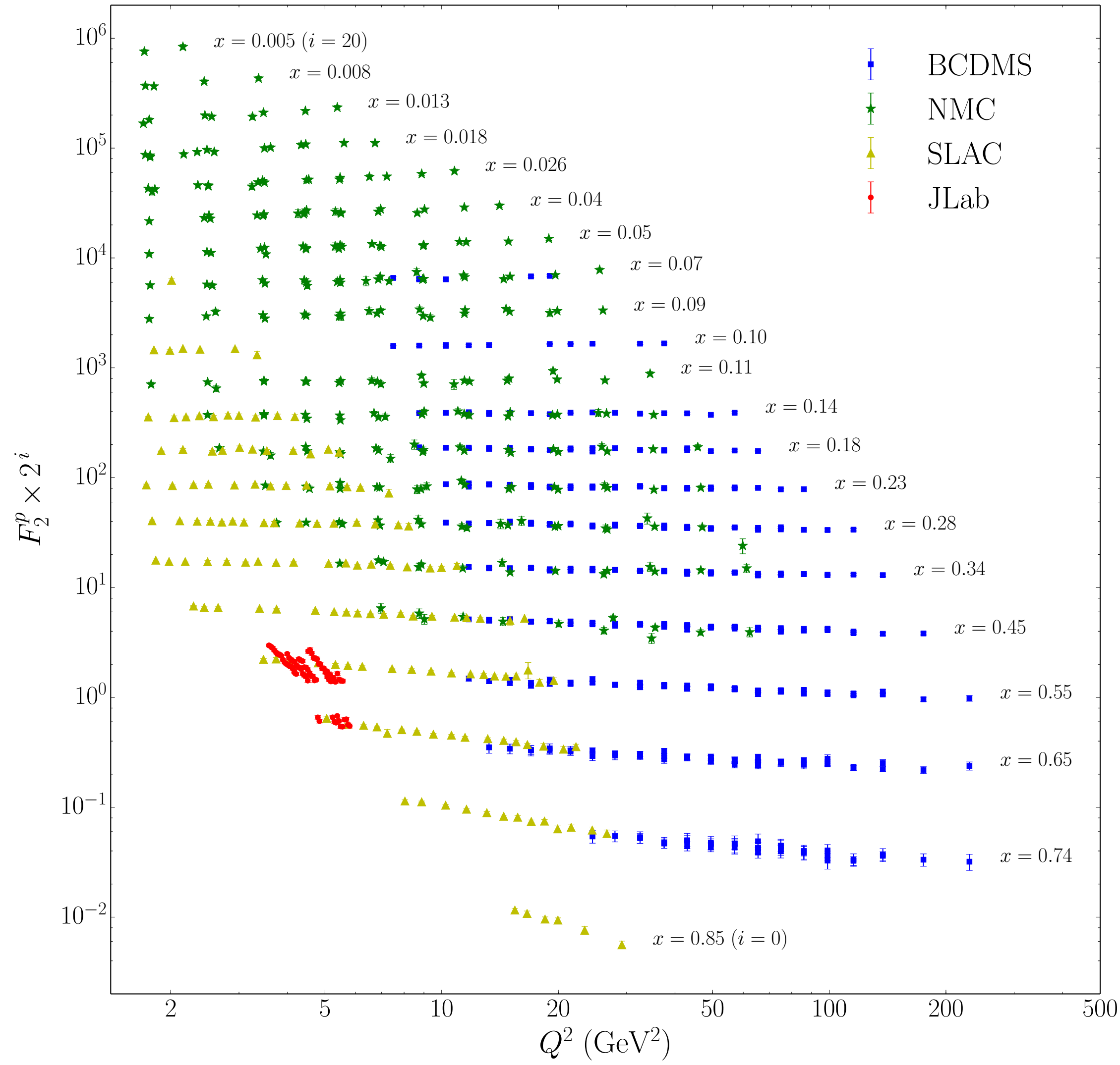

FIG. 1: Comparison of proton F_2^p structure function data from BCDMS [22], NMC [23], SLAC [25] and JLab [26] with the CJ15 NLO fit, for various Q^2 and x. The data at fixed x values have been scaled by a factor 2^i, from $i = 0$ for $x = 0.85$ to $i = 20$ for $x = 0.005$ in steps of $i = 1$.

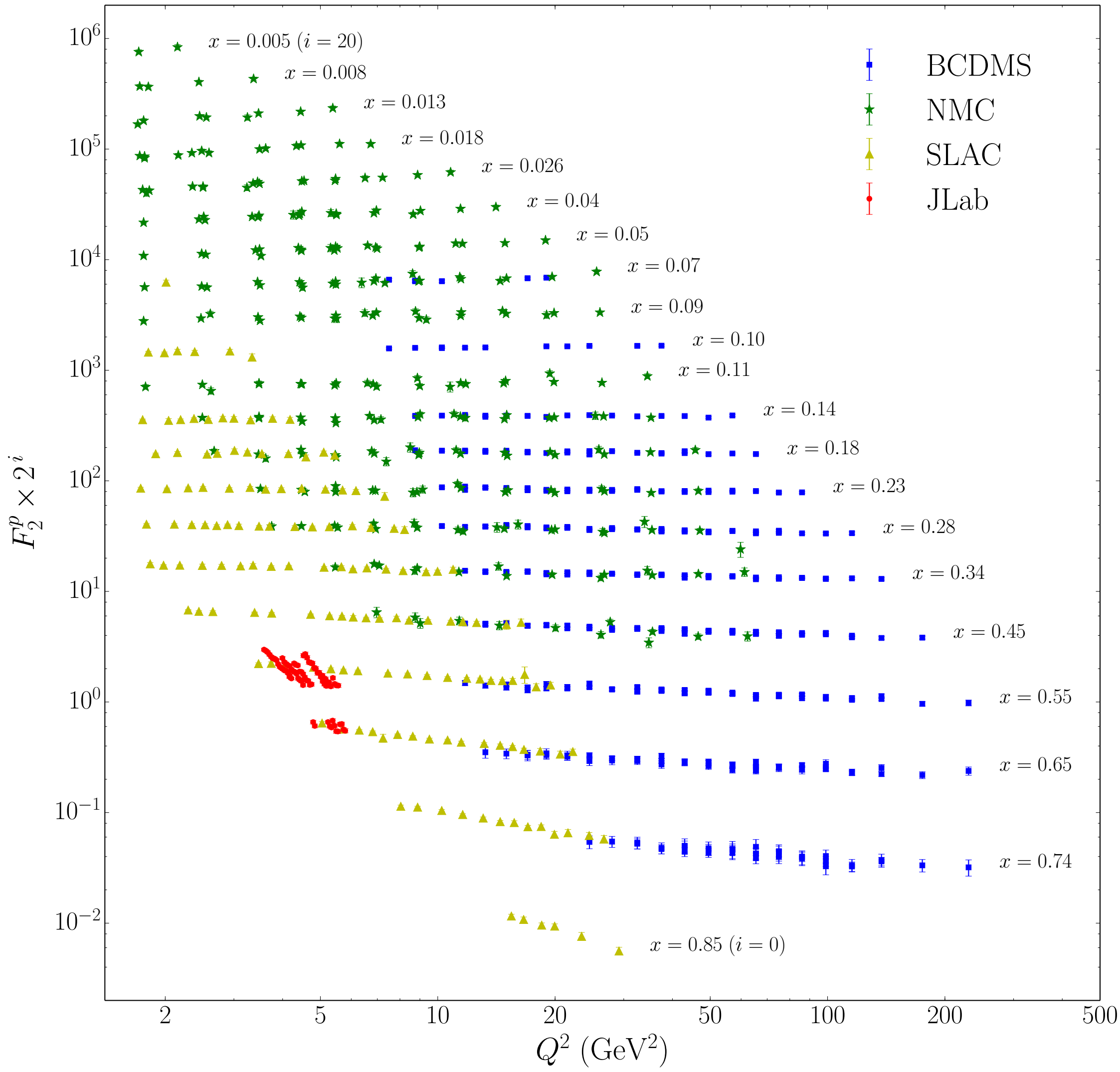

FIG. 2: [PLACEHOLDER FIGURE]... As for Fig. 1, but for the deuteron F_2^d structure function, illustrating data from BCDMS [22], SLAC [25] and JLab [26]. ...[WHAT TO DO WITH NMC F_2^d/F_2^p ?]...

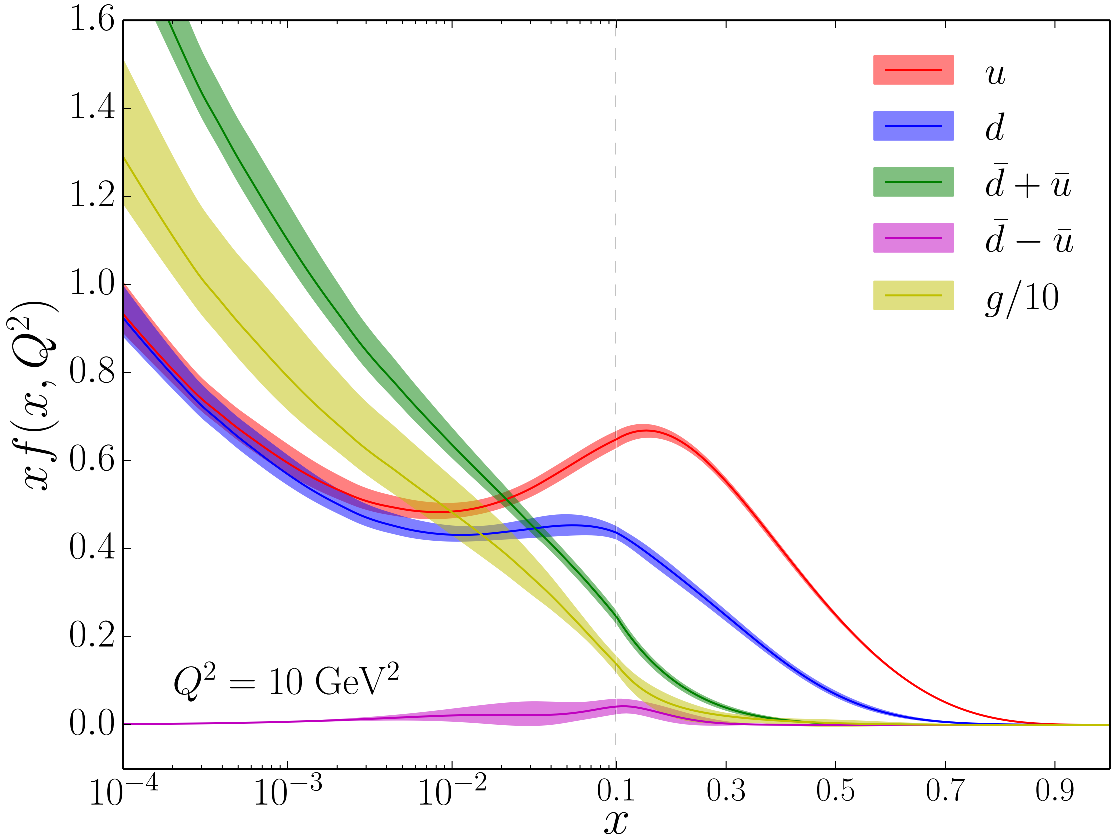

FIG. 3: Comparison of CJ15 PDFs for different flavors ($u, d, \bar{d}+\bar{u}, \bar{d}-\bar{u}$ and $g/10$) at a scale $Q^2 = 10$ GeV^2, for $T = 1$. Note the combined logarithimic/linear scale along the x-axis.

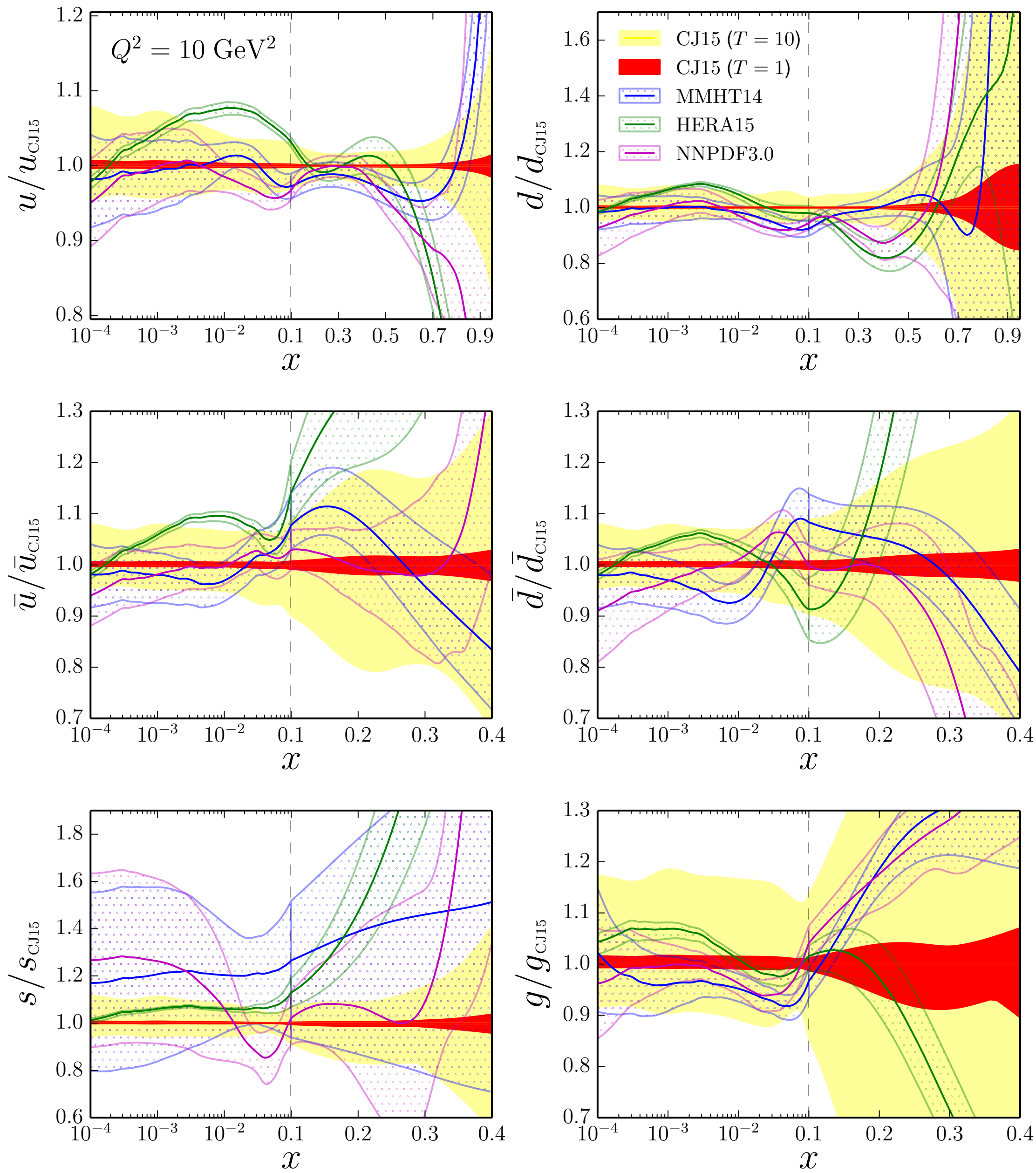

FIG. 4: Ratio of PDFs to the CJ15 central values for various PDF sets: CJ15 for tolerance $T = 1$ (red) and $T = 10$ (yellow), MMHT14 [17] (blue), HERAPDF15 [21] (green), and NNPDF3.0 [19] (magenta). Note the different scales on the vertical axes used for different flavors.

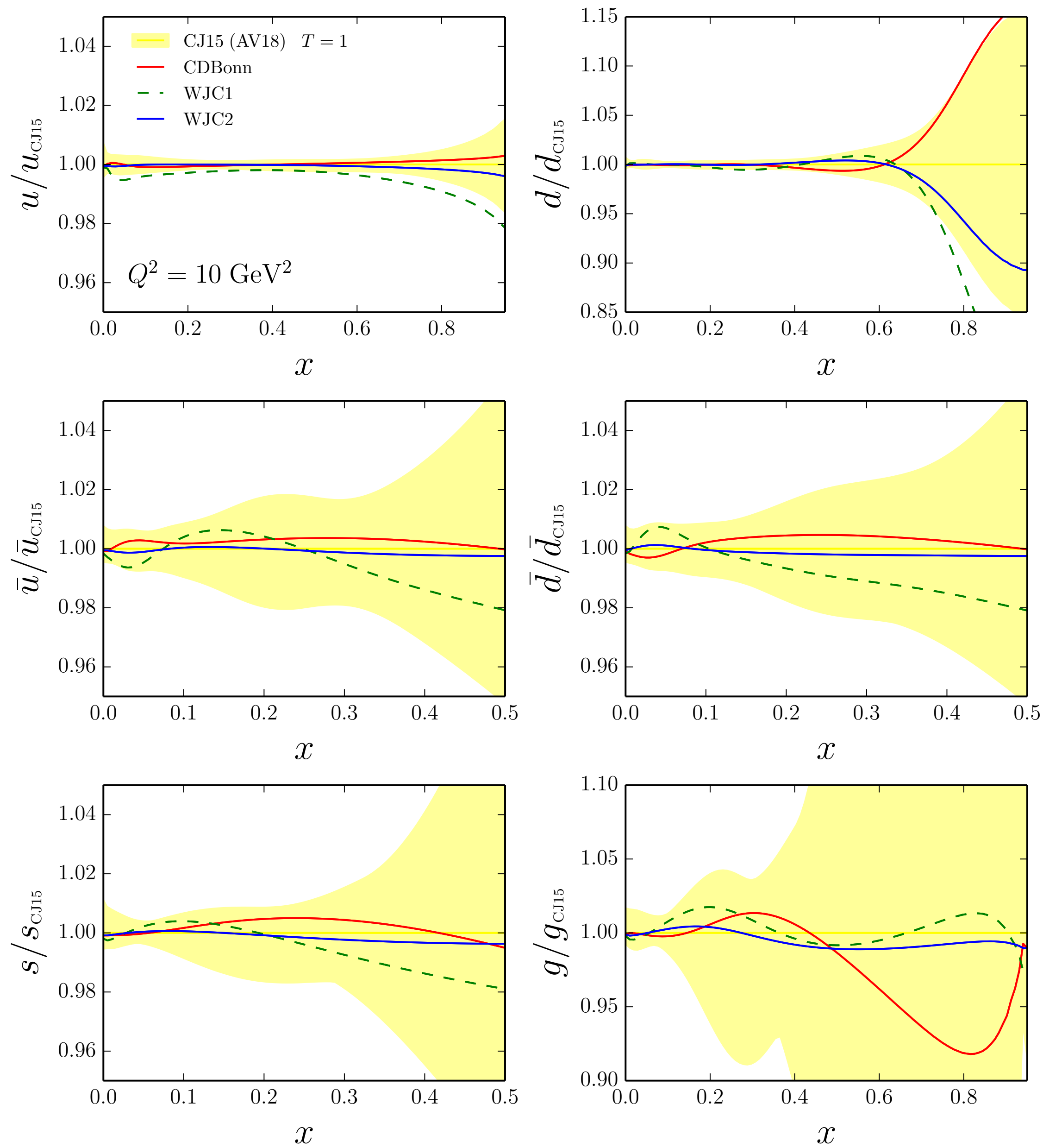

FIG. 5: Ratio of PDFs fitted using various deuteron wave function models to the CJ15 PDFs (which use the AV18 deuteron wave function): CD-Bonn (red solid lines), WJC-1 (green dashed lines), WJC-2 (blue solid lines). The CJ15 PDFs (yellow band) are shown for $T = 1$, and the off-shell parametrization (12) is used for all cases. Note the different scale on the vertical axes for the d-quark and gluon distributions.

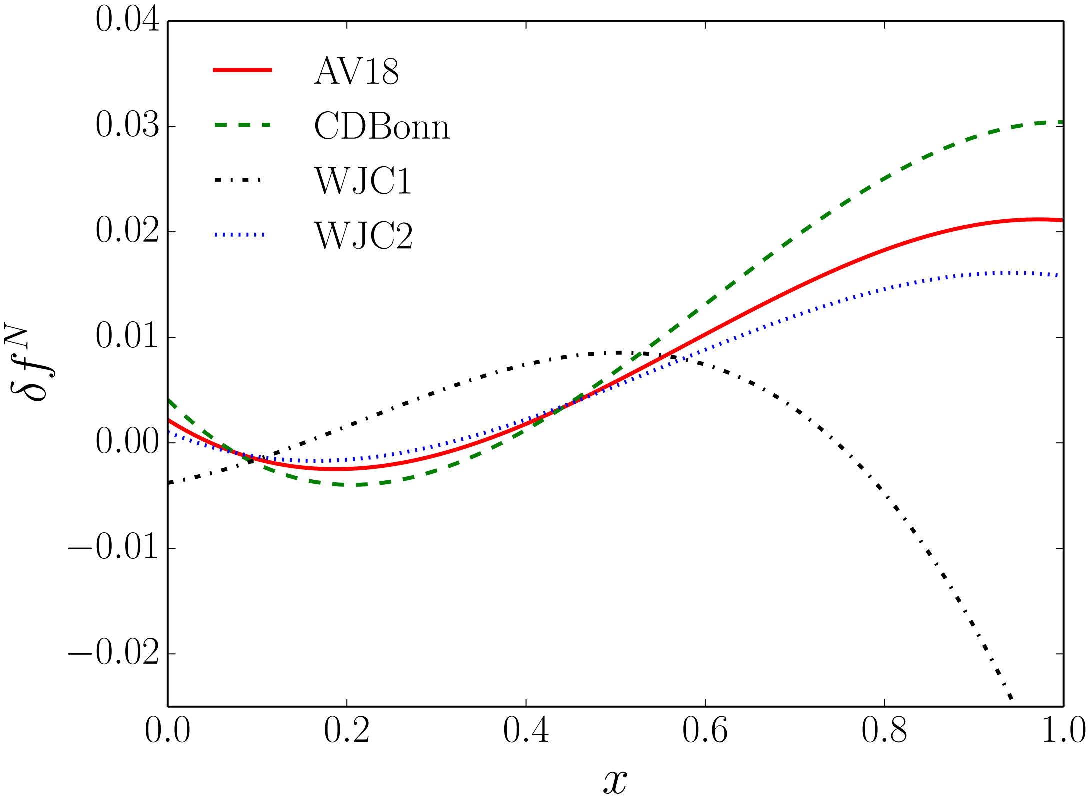

FIG. 6: Fitted nucleon off-shell correction δf^N for the parametrization in Eq. (12), using the AV18 (solid red line), CD-Bonn (dashed green line), WJC-1 (dot-dashed black line) and WJC-2 (dotted blue line) wave functions.

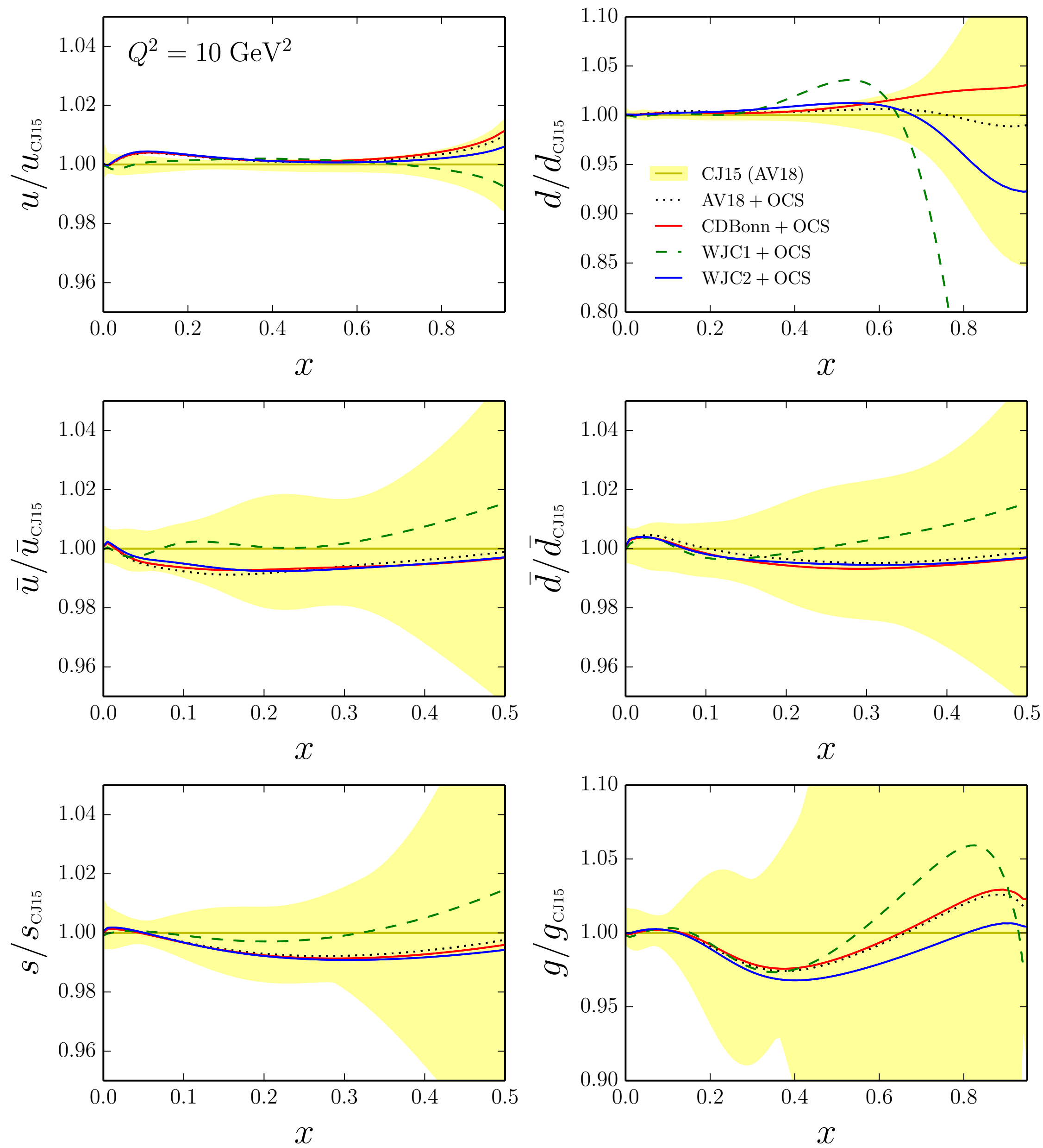

FIG. 7: Ratio of PDFs computed using the off-shell covariant spectator (OCS) model and different deuteron wave functions to the CJ15 PDFs (which use the off-shell parametrization (12) and the AV18 deuteron wave function): OCS model with the AV18 wave function (black dotted lines), CD-Bonn (red solid lines), WJC-1 (green dashed lines), and WJC-2 (blue solid lines). Note the different scale on the vertical axes for the d-quark and gluon distributions.

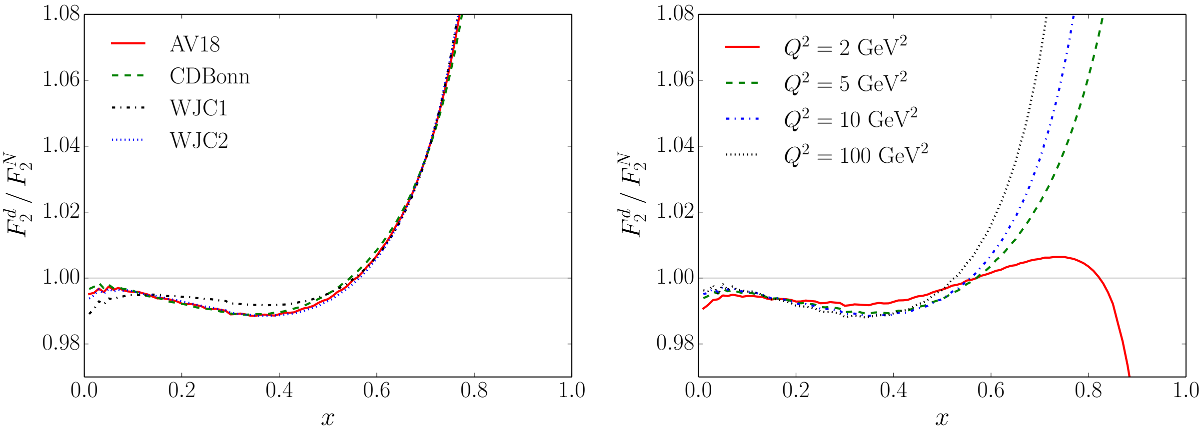

FIG. 8: Ratio of deuteron to isoscalar nucleon structure functions F_2^d/F_2^N for **(a)** different deuteron wave function models at $Q^2 = 10$ GeV^2, and **(b)** different values of Q^2 for the AV18 wave function.

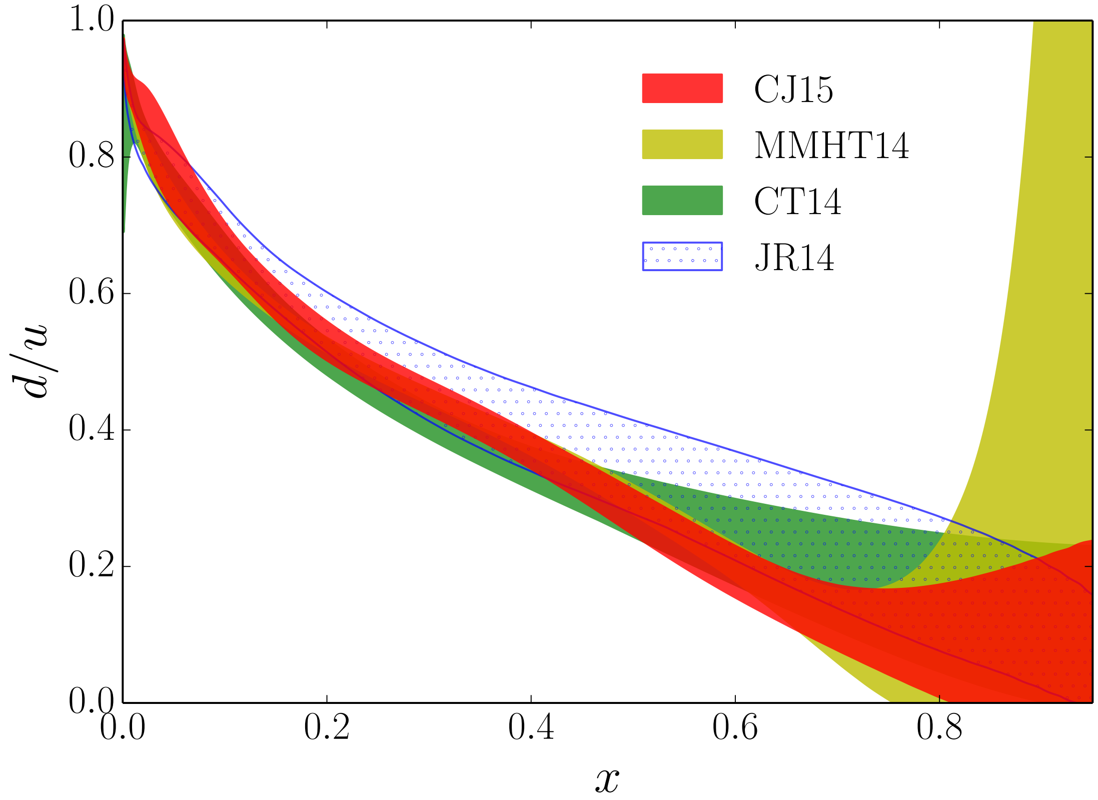

FIG. 9: Comparison of the d/u ratio at $Q^2 = 10$ GeV^2 for different PDF parametrizations: CJ15 (red band), MMHT14 [17] (yellow band), CT14 [18] (green band), and JR14 [47] (blue dotted band).

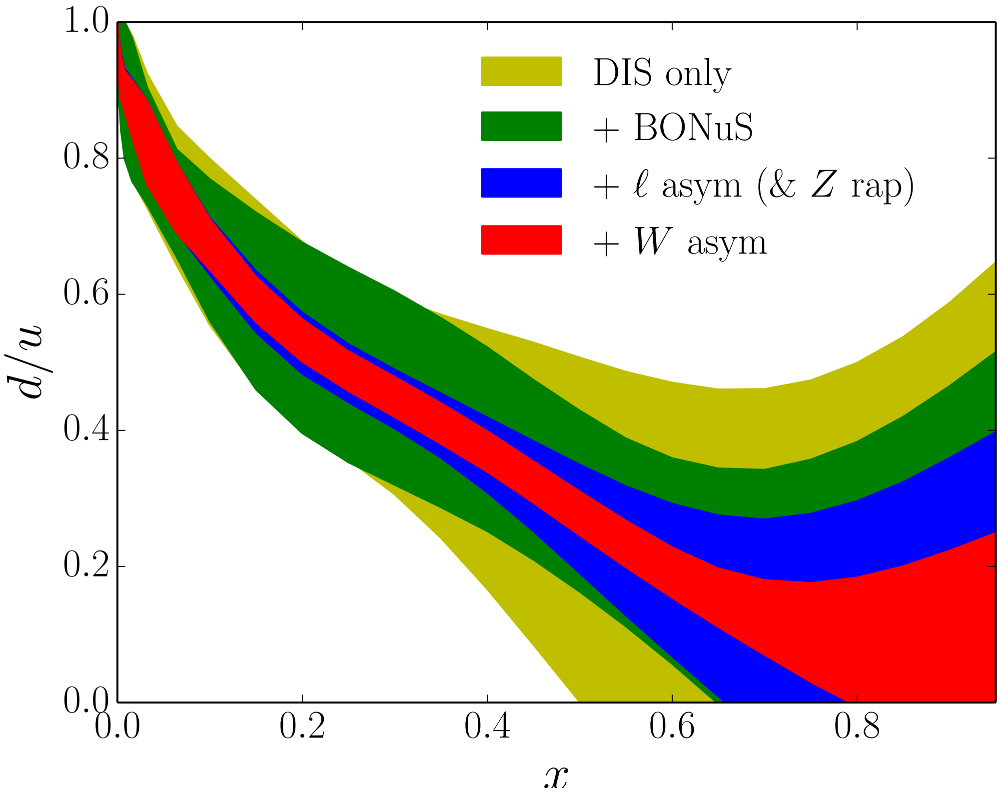

FIG. 10: Impact of various data sets on the d/u ratio at $Q^2 = 10$ GeV^2. The uncertainty band is largest for the DIS only data (yellow band), and decreases with the successive addition of JLab F_2^n/F_2^d [83] data (green band), lepton asymmetry [30–32] (and Z rapidity [35, 36]) data (blue band), and W boson asymmetry data [33, 34] (red band). ...[FIGURE NEEDS SMOOTHING]...

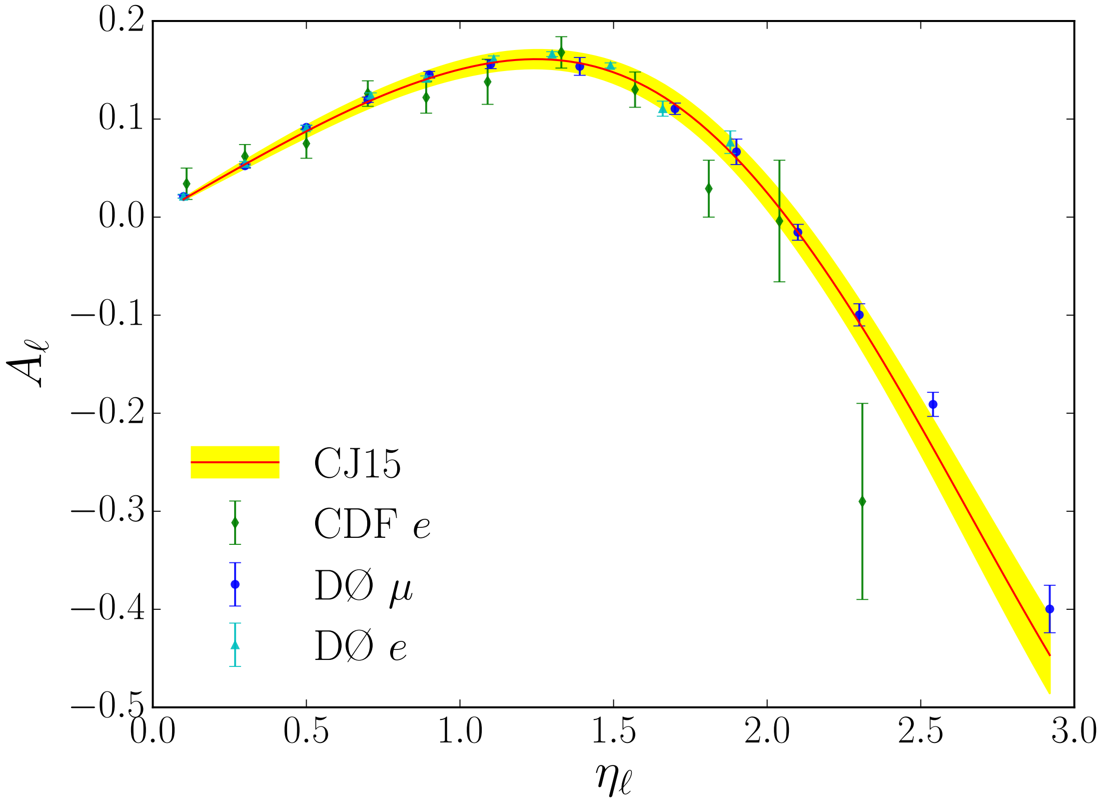

FIG. 11: Lepton charge asymmetry A_ℓ from $p\bar{p} \to WX \to \ell\nu X$ as a function of the lepton pseudorapidity η_ℓ from CDF electron (green diamonds) [30], and DØ muon (blue circles) [31] and electron (cyan triangles) [32] data compared with the CJ15 fit.

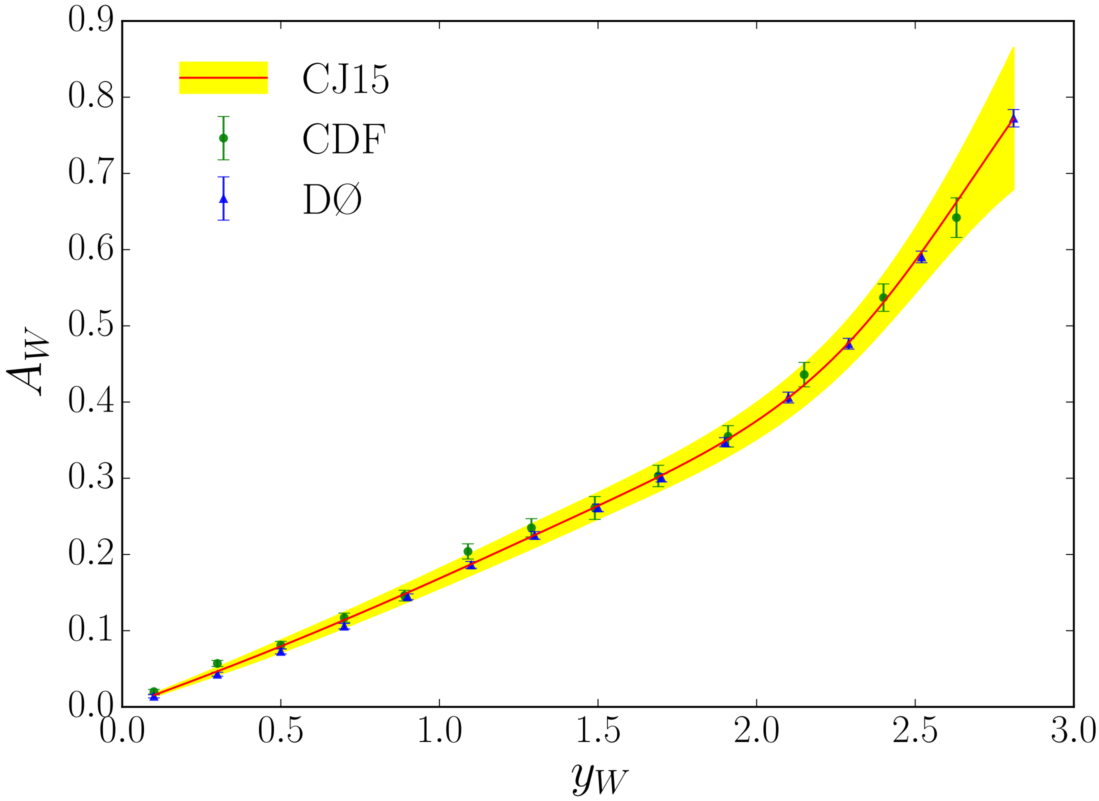

FIG. 12: W boson charge asymmetry A_W from $p\bar{p} \to WX$ as a function of the W boson rapidity y_W for CDF (green circles) [33] and DØ (blue triangles) [34] data compared with the CJ15 fit.

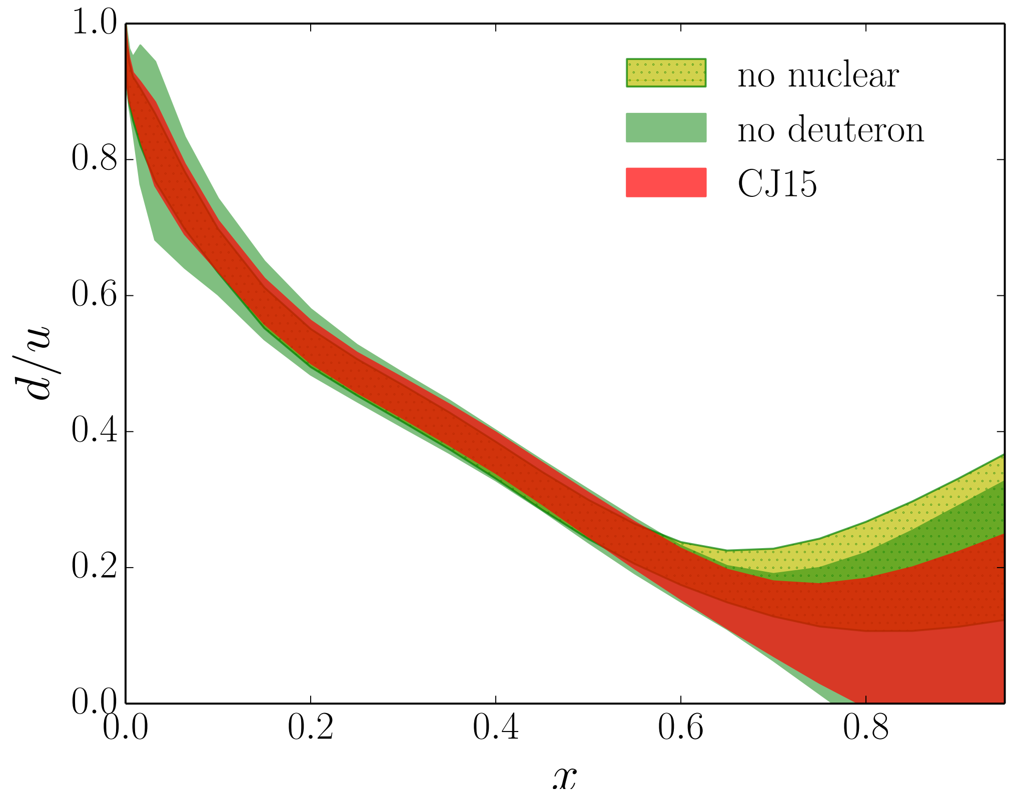

FIG. 13: Impact on the CJ15 d/u ratio (red band) of removing the deuterium nuclear corrections (yellow shaded band), and omitting the deuterium data (green band). ...[FIGURE NEEDS SMOOTHING]...

TABLE I: Data sets used in the CJ15 NLO global analysis (which uses the AV18 deuteron wave function and off-shell parametrization in Eq. (12), with the corresponding number of data points and the respective χ^2 values for each set. For comparison the χ^2 for the LO fit and for an NLO fit with the OCS off-shell model are also given.

	experiment	# points	χ^2		
			NLO	LO	NLO (OCS)
DIS F_2	BCDMS (p) [22]	351	437	432	435
	BCDMS (d) [22]	254	294	299	289
	NMC (p) [23]	275	407	414	406
	NMC (d/p) [24]	189	172	180	173
	SLAC (p) [25]	564	435	496	436
	SLAC (d) [25]	582	372	417	386
	JLab (p) [26]	136	166	164	166
	JLab (d) [26]	136	124	127	123
	JLab (n/d) [83]	191	217	224	215
DIS σ	HERA (NC e^-p) [27]	145	112	161	113
	HERA (NC e^+p) [27]	408	541	872	541
	HERA (CC e^-p) [27]	34	19	19	19
	HERA (CC e^+p) [27]	34	31	33	32
Drell-Yan	E605 (pCu) [44]	119	93	104	93
	E866 (pp) [28]	121	139	155	139
	E866 (pd) [28]	129	144	191	144
	E866 (pd/pp) [29]	12	9	9	8
W/charge asymmetry	CDF (e) [30]	11	12	11	12
	DØ (μ) [31]	10	20	21	29
	DØ (e) [32]	13	27	56	22
	CDF (W) [33]	13	15	12	15
	DØ (W) [34]	14	16	47	16
Z rapidity	CDF (Z) [35]	28	27	79	28
	DØ (Z) [36]	28	16	23	16
jet	CDF (run 2) [38]	72	15	22	15
	DØ (run 2) [40]	110	21	46	22
γ+jet	DØ 1 [41]	16	6	20	6
	DØ 2 [41]	16	15	40	15
	DØ 3 [41]	12	25	35	25
	DØ 4 [41]	12	13	77	13
total		4035	**3941**	4786	3952
total + norm			**3950**	4918	3961
χ^2/dof			**0.979**	1.219	0.982

TABLE II: Leading twist parameter values for the u_v, d_v, $\bar{d}+\bar{u}$, $\bar{d}-\bar{u}$ and g PDFs [Eq. (1)] from the CJ15 NLO analysis at the initial scale Q_0 GeV. Parameters without errors have been fixed. For the strange to non-strange sea quark PDF ratio [Eq. (4)], we take $\kappa = 0.4$. (The parameter values are given to 5 significant figures to avoid rounding errors.)

parameter	u_v	d_v	$\bar{d}+\bar{u}$	$\bar{d}-\bar{u}$	g
a_0	2.3585	23.233	0.14121 ± 0.0050459	35712	46.706
a_1	0.60985 ± 0.020299	1.1387 ± 0.034586	-0.21785 ± 0.0039454	3.9867 ± 0.049301	0.61586 ± 0.038277
a_2	3.5377 ± 0.011405	6.6180 ± 0.15977	8.4003 ± 0.14833	20.289 ± 0.66322	6.2335 ± 1.1222
a_3	0	-3.5743 ± 0.090782	0	17	-3.2703 ± 0.16746
a_4	3.5169 ± 0.42791	4.9133 ± 0.14586	16.055 ± 1.1403	49.881 ± 7.1398	3.0338 ± 0.31300
b	—	$-0.0042424 \pm 0.00070691$	—	—	—
c	—	2	—	—	—

TABLE III: Parameter values for the nucleon off-shell [Eq. (12)] and higher twist [Eq. (6)] corrections to F_2 from the CJ15 NLO analysis at the input scale Q_0^2. The off-shell parameters are fitted using the AV18 deuteron wave function. Parameters without errors have been fixed. (The parameter values are given to 5 significant figures to avoid rounding errors.)

parameter	value
C_0	0.098222 ± 0.028518
x_0	0.34487 ± 0.91982
x_1	0.048
h_0	-3.0094 ± 0.24080
h_1	1.7526 ± 0.10135
h_2	-2.0895 ± 0.026853